Photoluminescence from Er-doped Si-rich Si oxides deposited by magnetron sputtering in Ar or Ar+H_2 plasmas

C. L. Heng,[a] E. Chelomentsev, O. H. Y. Zalloum, J. Wojcik, and P. Mascher[b]
Department of Engineering Physics and Centre for Emerging Device Technologies, McMaster University, Hamilton, Ontario L8S 4K1, Canada

(Received 4 September 2008; accepted 10 November 2008; published 30 December 2008)

The authors have studied photoluminescence (PL) from Er-doped Si-rich Si oxide (SRSO) films deposited by magnetron sputtering of an Er+Si+SiO_2 composite target in Ar or Ar+H_2 ambients. When the samples were annealed in N_2, for the film grown in an Ar ambient, the PL annealing behaviors reveal that the emissions from the film are defect-related and that the Er^{3+} PL at 1.54 μm is possibly triggered by a defect-mediated energy transfer process; while for the films grown in an Ar+H_2 ambient, the emissions from the SRSO matrix are suppressed and the Er PL intensities increase significantly but differently dependent on the Ar:H_2 ratios during sputtering. After annealing the samples in an Ar+5%H_2 (FG) ambient, however, almost no Er PL was observed from the film grown in the Ar ambient, while the Er PL intensities of the films grown in the Ar+H_2 ambient increase further compared to those annealed in N_2. Fourier transform infrared spectroscopy shows that the absorption of the samples after FG annealing is weaker than after annealing in N_2. The PL properties have also been compared to those of a sample grown by plasma enhanced chemical vapor deposition. The roles of hydrogen during sputtering and postdeposition annealing are discussed. © *2009 American Vacuum Society.* [DOI: 10.1116/1.3043465]

I. INTRODUCTION

Erbium (Er)-doped silicon (Si)-rich Si oxide (Er-SRSO) has been studied intensively for applications in photonics and optoelectronics,[1] since the Er^{3+} ions' room-temperature photoluminescence (PL) at ~1.54 μm first was reported to be substantially stronger than that from Er-doped silica.[2] Various techniques have been employed independently or jointly to fabricate Er-SRSO thin films, such as ion implantation,[3–5] plasma-enhanced-chemical-vapor deposition (PECVD),[6–8] magnetron sputtering,[9–11] and laser ablation.[12,13] The excitation of Er^{3+} ions in the films is regarded to be initiated by an energy transfer from Si nanoclusters (Si-ncls) to nearby Er^{3+} ions. The efficiency of the Er PL depends on the details of Si-ncls. Amorphous Si-ncls as well as Si nanocrystals have been demonstrated to be efficient luminescence sensitizers.[14] Besides Si-ncls, defects due to excess Si in the SRSO matrix are also believed to act as sensitizers for the excitation of Er^{3+} ions.[15] The Er PL also depends on the concentration of Er, although only a small fraction of the Er^{3+} ions are optically active.[16,17] Moreover, for an Er-SRSO film with given concentrations of Si and Er, the Er PL efficiency can be influenced greatly by postdeposition annealing.[18] For undoped SRSO, Comedi *et al.*[19] reported that the emissions at wavelengths in a range of 780–950 nm can be enhanced greatly after annealing in forming gas Ar+5%H_2 (FG) ambient, with hydrogen passivating nonradiative recombination centers (i.e., dangling bonds) believed to be responsible for the enhancement. Gourbilleau *et al.*[20] annealed Er-SRSO films in N_2 or N_2 +5%H_2, and also suggested that the hydrogen passivating dangling bonds was responsible for the Er PL difference between the two gas ambients annealing. Previously,[18] we have suggested that when an Er-SRSO film was annealed in N_2 +H_2, Si oxynitrides form around Si-ncls, which hinders the energy transfer from Si-ncls to Er^{3+} ions, thus decreasing the Er PL efficiency. In this study, we have deposited the Er-SRSO films by magnetron sputtering of an Er+Si+SiO_2 composite target in Ar or Ar+H_2 ambients with different Ar:H_2 gas ratios, and studied the PL from the films annealed in N_2 and FG, respectively. We have also compared the PL efficiency to that of an Er-SRSO film grown by electron-cyclotron-resonance (ECR) PECVD.

II. EXPERIMENTAL DETAILS

Three Er-doped SRSO thin films (labeled as samples A, B, and C) were deposited on Si substrates by rf magnetron sputtering of an Er+Si+SiO_2 composite target consisting of small Si and metallic Er chips placed on a 2 in. SiO_2 plate (99.99% purity). The area ratio of Er to Si was 4.5:72.6. The base vacuum of the chamber was about 3×10^{-7} Torr. The films were deposited without any intentional heating of the substrates and with a power density of 6.41 W/cm^2. The working gas pressure during the deposition of samples A and B was 5.0×10^{-3} Torr but was 10.0×10^{-3} Torr for the deposition of sample C. Sample A was deposited by sputtering the target in a pure Ar ambient, while samples B and C were deposited by sputtering in Ar+H_2 ambients with Ar:H_2 gas flow ratios of 1:1 and 2.2:20, respectively. The as deposited (A.D.) samples were characterized by using ellipsometry with laser wavelength of 632.8 nm and Rutherford backscattering spectroscopy (RBS), the results of which are shown in Table I. The uncertainty of the RBS measurements is ~1 at. %. Our sample growth is well controlled and the

[a]Electronic mail: hengche@mcmaster.ca
[b]Electronic mail: mascher@mcmaster.ca

TABLE I. Characteristics and composition for samples A, B, C, and D.

Sample	Deposition method	Thickness (nm)	Refractive Index (at 632.8 nm)	Si concentration (at. %)	Er concentration (at. %)
A	Sputter in Ar	423.4 ± 19	1.52	32.8	1.43
B	Sputter in $Ar:H_2$ (1:1)	343.1 ± 12	1.66	35.5	1.21
C	Sputter in $Ar:H_2$ (2.2:20)	370.0 ± 12	1.63	33.9	1.06
D	ECR-PECVD	56 ± 2	1.83	44.7	1.20

reproducibility is very good. Under the same deposition conditions, the deposition rate of the growing film varies within 2 Å/min, and the refractive index varies by less than 0.02 from one sample to another. For comparison, another Er-doped SRSO film (sample D) was synthesized by using ECR-PECVD with an organic Er source supplying the *in situ* doping. The details of the film deposition can be found elsewhere.[6] The parameters of A.D. sample D are also shown in Table I. After the depositions, all the samples were cleaved into small pieces and subjected to thermal annealing treatments in flowing N_2 or FG ambients for 30 min at different temperatures as indicated in the text.

Fourier transform infrared (FTIR) spectroscopy was used to study the structural changes in the annealed samples by employing a Bio-Rad FTS-40 instrument with a resolution of 4 cm^{-1}. The attenuated total reflection (ATR) technique was employed by using a special attachment with a 45° incident angle. The advantage of this technique comes from the multiple internal reflections that take place in the crystal. As the refractive index of the deposited films is much smaller than that of the ATR crystal, only evanescent waves penetrate into the grown film. For our cases, the total number of internal reflections is calculated to be about 16, resulting in enhanced absorption spectra. The PL was excited with an unfocused beam (~1 mm diameter) using the 325 nm line of a He–Cd laser with a nominal power of 17 mW (note that the 325 nm exciting line is nonresonant with the excitation of Er ions). The PL spectra in the 1400–1700 nm range were measured using a 500 mm grating monochromator (3 mm slits), a lock-in amplifier with a chopper working at 40 Hz, and an InGaAs detector. The PL spectra in the 350–900 nm range were measured using a charge coupled device based spectrometer. The effective power density of the laser beam on the surface of the samples was ~0.64 W/cm^2, corresponding to a photon flux of 1.05×10^{18} cm^{-2} s^{-1}; while for the IR measurement, the photon flux after the chopper and two reflective mirrors could be as little as half of this value. The visible PL spectra were corrected for system response and optics transmission and subsequently converted to, and presented in normalized photon flux (arbitrary units). All the measurements were performed at room temperature.

III. RESULTS AND DISCUSSION

From Table I, it can be seen that by increasing the H_2 partial pressure upon sputtering, the Si concentration (refractive index) in the final films first increases from 32.8 (1.52) to 35.5 at. % (1.66) then decreases to 33.9 at. % (1.63), while the Er concentration decreases monotonically from 1.43 to 1.06 at. %. The increase in Si content after the $Ar+H_2$ sputtering, should be due to hydrogen chemically reducing in the plasma the oxygen from the sputtered target.[21] However, Si atoms from the growing film surface can also react with hydrogen to form volatile species (such as SiH_4 or Si_2H_6) and then being pumped away. So, there exists an optimum H_2 partial pressure for sputtering in $Ar+H_2$ gas ambient from which the Si concentration in the film can be maximized. It has been reported that when the partial pressure ratio of H_2 to Ar is 1:1, one can obtain the highest Si concentration in the film from a given $Er+Si+SiO_2$ composition target.[11] Below this ratio, hydrogen chemically reducing oxygen plays the major role and the Si concentration increases with increasing hydrogen partial pressure; above this ratio, hydrogen reacting with Si dominates and the Si concentration starts to decrease.

Figures 1(a) and 1(b) show the PL spectra of sample A A.D. or annealed in N_2 for 30 min at the temperatures as is indicated. The PL spectra shown in Fig. 1(a) are in the range of 350–850 nm indicative of the luminescence from the SRSO matrix of the film. The A.D. sample shows emission with a broad peak located at around 570 nm. After 600 °C

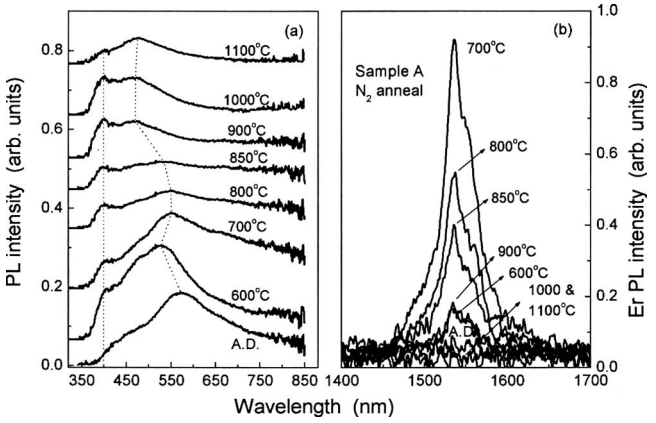

FIG. 1. PL spectra of sample A, as-deposied (A.D.) or annealed in N_2 for 30 min at 600, 700, 800, 850, 900, 1000, and 1100 °C, respectively: (a) the spectra in the range of 350–800 nm indicative of the emission from the SRSO matrix of the film and (b) the Er^{3+} PL at ~1.54 μm. The base lines of the spectra were shifted for clarity.

annealing the peak position shifts to ~526 nm and a shoulder at ~400 nm emerges in the spectrum. The peak position is at ~550 nm after 700 °C annealing and shifts with increasing the temperature to ~470 nm after 900 °C annealing. As the temperature increases further to 1100 °C, the 470 nm peak position remains almost the same. Note that the 400 nm shoulder is almost unchanged at all the temperatures. Figure 1(b) shows the Er^{3+} PL spectra at ~1.54 μm for the above annealed sample A. The Er PL from the A.D. sample is very weak, but becomes evident after 600 °C annealing. The PL intensity increases drastically and reaches the maximum value after 700 °C annealing. Further increasing the annealing temperature causes the PL intensity to decrease and after 1000 and 1100 °C annealing, almost no Er emission was observed.

From the annealing behaviors of the emission bands, we believe that the bands originate from defects (or impurities) rather than from Si-ncls. A 400 nm emission reported in silica implanted with Si ions was associated with B_2 centers (O≡Si—Si≡O) (Refs. 22 and 23) since oxygen vacancies can be generated by Si ions impinging on the SiO_2 network and one oxygen vacancy will generate two kinds of defects: E' (O≡Si∗) and the B_2 centers depending on its electronic charge. For the 400 nm band (or shoulder) present here, we believe that oxygen vacancies can be created in our film and form the B_2 centers upon the incorporation of Er. We suggest that there are at least two types of defects responsible for the emission bands lying between 470 and 570 nm: one type of defect has emissions at around 470 nm and the other emits at ~570 nm. The 470 nm component can be attributed to oxygen vacancy type defects, such as neutral oxygen vacancies,[24,25] but the origin of the 570 nm component has various explanations in the literature, such as certain transitions in the oxide matrix,[26] or "extended defects."[27] Then the decrease in the PL intensity is due to the amount of defects generally decreasing with increasing annealing temperature. The variation of the major peak position with increasing temperature is also attributed to the decrease in the defect concentrations but not at the same rate. Some defects vanish at lower temperatures while others can persist up to 1100 °C annealing. The change in the ratios among these defects leads to the peak position varying with the annealing temperature.

Note that after annealing at 700 °C the emissions at longer wavelengths of the spectrum (>700 nm) in Fig. 1(a) are becoming evident and correspond to the strongest Er PL [Fig. 1(b)]. One may suggest that Si-ncls have formed in the sample and acted as sensitizers for the Er PL. However, due to the Si:O ratio in sample A being very close to stoichiometric, it is less likely that the drastic variation of the Er PL intensities is caused by precipitation of Si-ncls and their density varying upon annealing from 600 to 900 °C. Also note that when the Er PL reaches the maximum intensity after 700 °C annealing, the corresponding major peak [Fig. 1(a)] is located at ~550 nm. It is well known that Er^{3+} ions can have visible emissions at 391, 408, 441, and 550 nm, which correspond to the optical transitions from $^4G_{11/2}$, $^2H_{9/2}$, $^4F_{3/2}$,

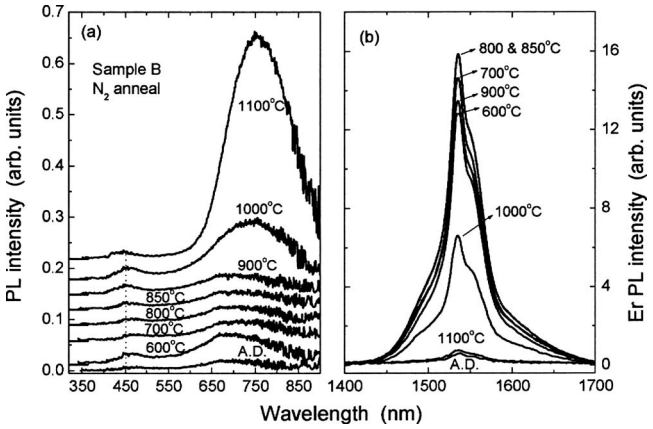

FIG. 2. PL spectra of sample B as-deposited or annealed in N_2 for 30 min with increasing the temperature from 600 to 1100 °C: (a) from the SRSO matrix and (b) the Er^{3+} 1.54 μm PL. The base lines of the spectra were shifted for clarity.

and $^4S_{3/2}$ energy levels to the ground level ($^4I_{15/2}$), respectively. Then the maximum Er PL is likely due to the Er^{3+} ions being resonantly excited by the defects' luminescence through a fluorescence resonance energy transfer process, i.e., the photons emitted from the defect will be absorbed by an Er^{3+} ion to excite an electron from the $^4I_{15/2}$ level to the $^4S_{3/2}$ level. The electron then will relax to the $^4I_{13/2}$ level, and finally decay back to the $^4I_{15/2}$ level to emit a photon with 1.54 μm wavelength. This indicates a defect-related energy transfer process for the excitation of Er^{3+} ions, which has been reported by Kozanecki *et al.* as a major energy transfer mechanism in Er-doped SRSO film.[15,28] After annealing at higher temperatures (800–850 °C), the amount of the defects decreases, and their emission wavelengths deviate gradually from the resonant excitation wavelength, so the Er PL at 1.54 μm decreases.

Figures 2(a) and 2(b) show the PL spectra of the SRSO matrix and the Er PL for sample B, which was annealed under identical conditions as sample A. In Fig. 2(a), there are two emission bands present in the spectrum of the A.D. sample: one weak band has a peak position at ~450 nm and another broadband has a peak position at ~680 nm. The PL intensity again increases after 600 °C annealing, but decreases with further increasing the annealing temperature to 900 °C. The peak position of the 680 nm band does not change upon these annealing temperatures, but the PL intensities (from the 680 nm band) are obviously weaker than those of sample A. The intensity has a higher value after 1000 °C annealing and the peak position redshifts to ~740 nm. After 1100 °C annealing, the peak position redshifts slightly (~750 nm) while the PL intensity shows a significant enhancement. Note that the 450 nm band remains weak and almost unchanged at all annealing temperatures. In Fig. 2(b), the Er PL from the A.D. sample B is rather weak, but the intensity shows a significant increase after the 600 °C annealing. Then the Er PL intensity increases further with increasing temperature and reaches a maximum value at 800 and 850 °C. Beyond this, the intensity starts to decrease

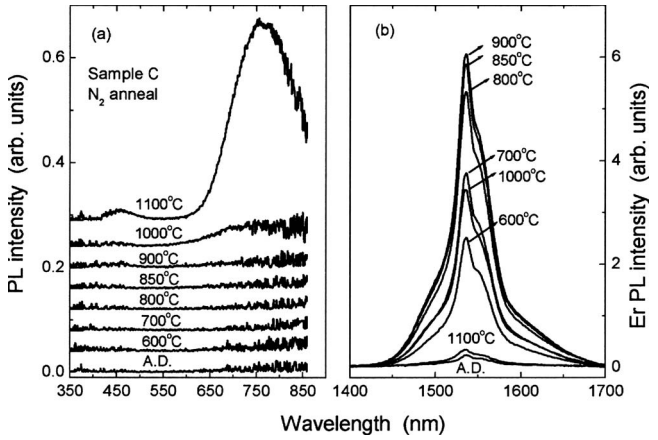

FIG. 3. PL spectra for sample C as-deposited or annealed in N_2 for 30 min at elevated temperatures from 600 to 1100 °C: (a) from the SRSO matrix (b) the Er^{3+} 1.54 μm PL. The base lines of the spectra were shifted for clarity.

with increasing temperature. The intensity is 87% of the maximum value after 900 °C annealing, only 42% after 1000 °C annealing and is very weak again after the 1100 °C annealing.

The ~450 nm band likely originates from oxygen deficient centers (ODCs),[29] which are normally regarded to be responsible for the short-wavelength emission. The ~680 nm (or longer) emissions should be mainly related to the radiative recombination within very small Si-ncls, the broad emission band may also include the contribution from certain defects, for example, nonbridging oxygen hole centers which have emission wavelengths at around 650 nm.[30] After 600 °C annealing, more Si-ncls have formed in the sample and act as efficient sensitizers of the Er^{3+} ions, so the Er PL increases significantly. The decrease in the emission from the SRSO matrix with further increasing the annealing temperature is likely due to the defects being gradually annealed out; the coupling between Si-ncls and Er atoms also quenches the emission from the Si-ncls. When annealing at even higher temperatures (1000 and 1100 °C), the redshift of the major peak position could be related to an increase in the size of the Si-ncls (an increase in Si-ncls' size after annealing at high temperature was observed by transmission electron microcopy[31]); and the significant increase in the PL intensity is due to crystallized Si-ncls being formed which have much higher emission efficiency than amorphous Si-ncls.[32,33] The decrease in the Er PL after annealing at temperatures higher than 900 °C [Fig. 2(b)], likely is also due to an increase of Si-ncls' size and the formation of Er-related precipitates in the film.[1]

Figures 3(a) and 3(b) show the PL spectra for sample C after identical thermal treatments. In Fig. 3(a), again, the PL from the SRSO matrix of the film is very weak, and almost no light emission was observed when the annealing temperature was lower than 1000 °C. Annealing at 1000 °C causes enhanced emissions at longer wavelengths (>680 nm) of the spectrum. After 1100 °C annealing, a strong broad emission band was observed with a peak wavelength at ~760 nm, and a weak band with peak position at ~450 nm emerges. In Fig. 3(b), similar to that shown in Fig. 2(b), the Er PL from the A.D. sample is rather weak, and after the 600 °C annealing the Er PL becomes quite strong. With further increasing the annealing temperature, the Er PL reaches a maximum intensity at about 900 °C, beyond which the PL intensity decreases with increasing the temperature up to 1100 °C.

From the PL spectra of the above three samples, it can be seen that by incorporating H_2 during the Ar sputtering, the defect-related emissions are greatly suppressed and the Er PL intensity increases significantly. After normalizing for the films thickness, we find that the maximum Er PL intensity of sample B is about 18.5 times stronger than that of sample A, and 1.4 times stronger than that of sample C. The significant enhancements of the Er PL are likely due to hydrogen passivation of dangling bonds at the interface of Si-ncl/SiO_2 which improves the radiative recombination within Si-ncls. Thus, more optical energy can be transferred from Si-ncls to Er^{3+} ions. The enhancements of the Er PL strongly depend on the Ar:H_2 ratio during the Ar+H_2 sputtering: a high H_2 partial pressure during Ar sputtering reduces the improvement of the Er PL.

Previously, we have demonstrated that PL spectra of Er-doped SRSO can be influenced significantly by post-deposition annealing in H_2-containing gas ambients.[18] However, annealing in N_2+H_2 was supposed to form Si oxynitride at the surface of Si-ncls, which hinders the energy transfer from Si-ncls to Er^{3+} ions.[31] Here, we have annealed samples A, B, and C in FG ambient for 30 min at their optimum temperatures for Er PL upon annealing in N_2 (700, 800, and 900 °C, respectively), and the PL spectra are shown in Figs. 4(a)–4(f). In Fig. 4(a), it can be seen that for sample A annealed in FG, the PL intensity of the SRSO matrix increases only slightly but the major peak position blueshifts from 550 to 470 nm, and the longer wavelength part of the spectrum decreases when compared to the case of annealing in N_2. The shift of the peak position is likely due to defects responsible for the 570 nm emission being sensitive to H_2 annealing and thus being passivated. From the temperature dependence of the defect-related PL [Fig. 1(a)] and the defect sensitivity to H_2 annealing, we believe that the defect is not likely to be an extended defect as was suggested in Ref. 27. The exact nature, however, is not clear at present. The decrease in the longer wavelength emission indicates that few Si-ncls are being formed upon the FG annealing. In Fig. 4(b), after annealing sample B in FG, both the 450 nm band and the 680 nm band have increased in intensity by about 17% compared to the case of N_2 annealing, the longer wavelength emission are also enhanced. Similar effects were observed for sample C after 900 °C annealing in FG as is shown in Fig. 4(c). The observed PL intensity increases slightly when compared to the case of 900 °C annealing in N_2. The influences of annealing in FG on the Er PL are shown in Figs. 4(d)–4(f). It can be seen [Fig. 4(d)] that for sample A after annealing in FG, almost no Er PL is observed. This indicates again that the Er PL in sample A more likely originates from a defect-related energy transfer process than from a Si-ncls-mediated transfer process. Figures 4(e) and

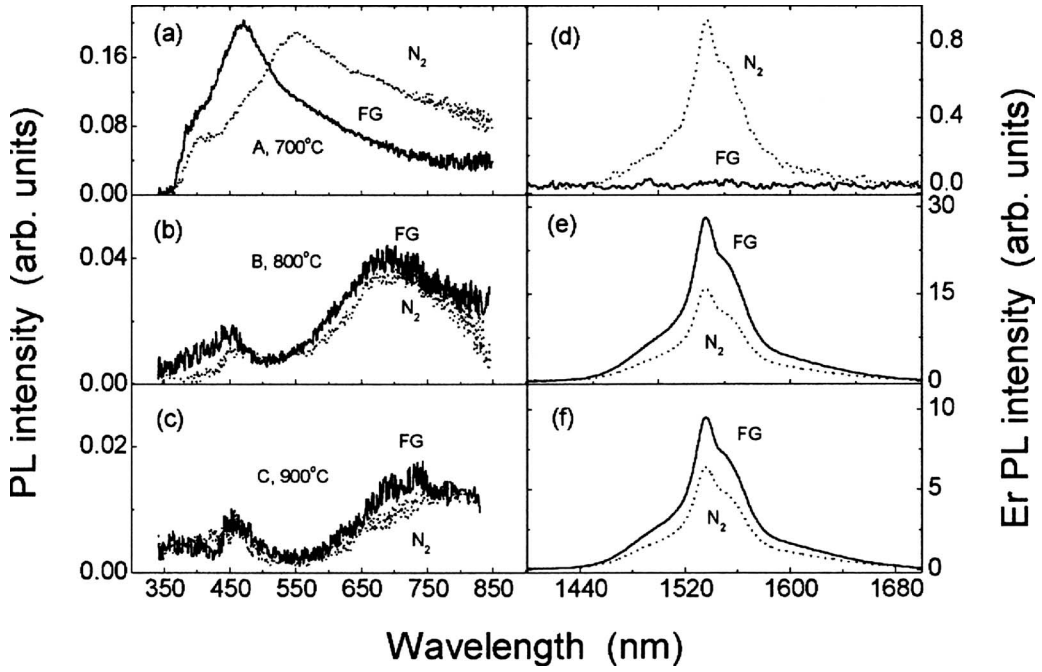

FIG. 4. PL spectra of the samples A, B, and C, annealed in FG for 30 min at the temperatures of 700, 800, and 900 °C, respectively: [(a)–(c)] from the SRSO matrix and [(d)–(f)] the Er^{3+} 1.54 μm PL. The PL spectra for the samples annealed in N_2 cases have been plotted in dotted lines for comparison.

4(f) show that the Er PL intensities of samples B and C after the annealing in FG have increased by 77% and 48%, respectively, compared to the cases of annealing in N_2. In summary, annealing in FG ambient significantly improves the Er PL efficiency but the enhancement also depends on the hydrogen partial pressure during the deposition.

The structural differences between samples A, B, and C annealed in N_2 and FG at their optimum temperatures for Er PL, have been studied by FTIR, the results of which are shown in Fig. 5. For sample A annealed at 700 °C in N_2, there are three major features present in the spectrum with peak positions at ~1110, ~996, and ~783 cm^{-1}, respectively. The three bands become less defined after annealing in FG and the 783 cm^{-1} band decreases the most in intensity. The 1110 cm^{-1} absorption band stems from the asymmetric (or out-of-phase) Si—O stretching vibration.[34,35] The 996 cm^{-1} band can be ascribed to the Si—O—Si stretching mode (it should be noted that with increasing the annealing temperature from room temperature to 1100 °C, the peak position of the band blueshifts from 992 to 1017 cm^{-1}, not shown). However, if we attribute the 996 cm^{-1} band only to the symmetric Si—O bonds, the [O]/[Si] atom ratio in sample A should be at ~0.66 (Ref. 36) or ~1.0, (Ref. 37) both of which are much lower than that obtained from our RBS analysis. We believe that upon the N_2 annealing some other chemical bonds, for example, Si—N bonds,[35] have formed and contributed to the wide band, as N can diffuse into the film and passivate the Si dangling bonds.[38,39] The 783 cm^{-1} band can be ascribed to both the Si—O bending mode and the Si—N stretching mode.[35,40] The decrease in the absorption after annealing the sample in FG is likely due to few Si—N bonds being formed. Hydrogen incorporation can either passivate the defects which emit light at around 550 nm or form O—H bonds[35] (the undesirable OH group quenches the Er PL greatly). So, the fact that almost no Er PL was observed after 700 °C annealing in FG can be understood.

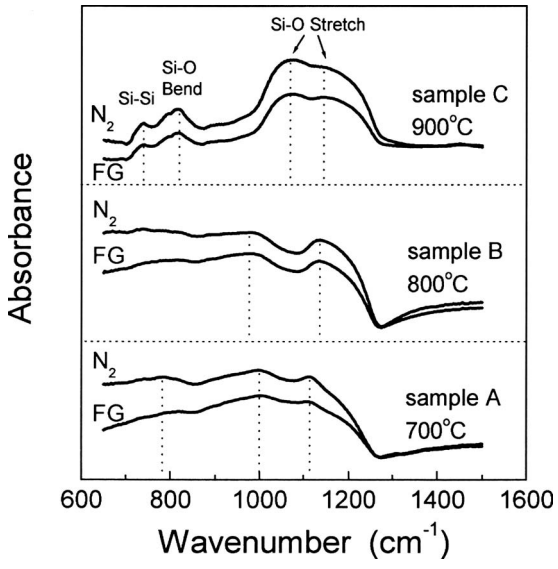

FIG. 5. FTIR spectra of samples A, B, and C, annealed in N_2 (or FG) for 30 min at the temperatures of 700, 800, and 900 °C, respectively.

For sample B annealed at 800 °C in N_2, similar three absorption bands are present in the spectrum, also shown in Fig. 5, with peak positions located at ~1135 and ~976 cm^{-1}, respectively, but the band in a range of 700–850 cm^{-1} is less defined. After annealing in FG, the absorption of the sample again decreases but the peak posi-

tions remain the same. Gourbilleau *et al.*[11] reported that the relative intensity of the longitudinal optical (LO_3) mode ($\sim$1250 cm^{-1}) for the Si—O vibrational mode with respect to the transversal optic (TO_3) mode ($\sim$1080 cm^{-1}), increases with increasing hydrogen partial pressure upon an $Ar+H_2$ sputtering, and suggested that this was a signature of the increase of interfacial silica, i.e., Si/SiO_2 surface, at the expense of volumic silica, which is induced either by the increase in Si excess for a given size of Si-ncls or by the increase in the density of small nanoclusters for a given value of Si excess. Therefore, we believe that the here observed changes in the shape of the $\sim$1135 cm^{-1} band are related to more Si-ncls being formed since more Si excess exists in sample B than in sample A. However, we cannot rule out the possibility that N—H bonds are being formed in the sample upon annealing in N_2, as the N—H bending mode can have frequencies ranging from 1150 to 1200 cm^{-1}.[35,41,42] The wide 976 cm^{-1} band is believed to be mainly from the Si—O—Si stretching mode (it should be noted that the peak position of the band blueshifts from 973 to 1001 cm^{-1} with increasing the annealing temperature from 25 to 1100 °C, not shown); however, the band may also include the contribution from the Si—H bending vibration since hydrogen is believed to have incorporated in the film and can have an absorption peak at $\sim$976 cm^{-1}.[36] In the case of FG annealing, again the decreases of the 1135, 976, and the 700–850 cm^{-1} absorption bands are likely due to less Si—N or N—H bonds being formed. The significant enhancement of the Er PL after annealing in FG is due to hydrogen passivating the Si dangling bonds and fewer chemical bonds (i.e., Si—N or N—H bonds) being formed at the surface of Si-ncls, both of which greatly improves the energy transfer efficiency.

The absorption spectra of sample C annealed at 900 °C are quite different from those of samples A and B. Four absorption features are present in the spectrum after annealing in N_2. The major band is located at around 1070 cm^{-1} with a shoulder at around 1145 cm^{-1}, and another two small absorption bands emerge with peak positions at $\sim$739 and $\sim$818 cm^{-1}, respectively. After annealing in FG, the 1070 cm^{-1} band decreases in intensity, and the shoulder evolves into a band with a peak position located at $\sim$1144 cm^{-1}. The two small bands also decrease in intensity but the peak positions are unchanged. The 1070 cm^{-1} peak in the spectra is attributed to the Si—O—Si stretching mode.[35,36] The $\sim$739 cm^{-1} peak can be ascribed to Si—Si bonds[43] or Si—N bonds, while the 818 cm^{-1} peak is likely due to the Si—O bending modes. Note that there is no indication of $Si—H_x$ bonds present in the spectra, which means that the hydrogen content in sample C is quite low. A decrease in the hydrogen content after magnetron sputtering at high H_2 gas flow rates was reported in amorphous hydrogenated Si film deposition, and attributed to "excessive hydrogen atoms in the gas phase extracting hydrogen from the surface of the depositing films."[44] We believe that a similar phenomenon has occurred during the film C deposition, the hydrogen incorporated in the film is low and not reflected in the FTIR spectra. After annealing in FG, the decreases in the absorption bands are again due to less Si—O bonds being formed, which improves the energy transfer from Si-ncls to Er^{3+} ions.

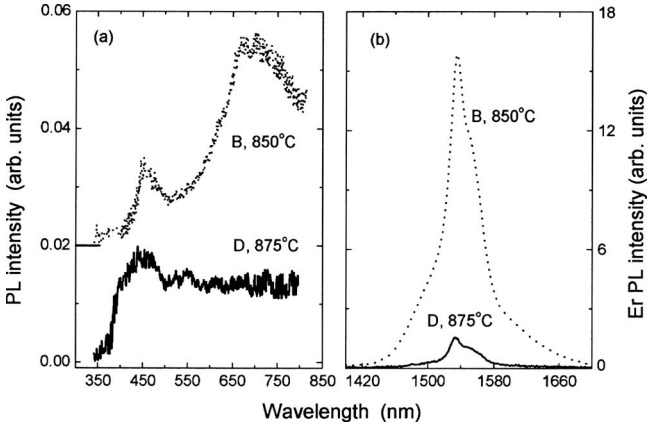

FIG. 6. Comparison of the PL spectra of samples B and D: (a) from the SRSO matrix and (b) the Er^{3+} 1.54 μm PL. Samples B and D were annealed in N_2 for 30 min at the temperatures of 850 and 875 °C, respectively.

Figure 6 show a comparison of the PL spectra of samples B and D, since the two samples have similar Er concentrations ($\sim$1.2 at. %) but different Si excess (35.5 at. % versus 44.7 at. %). Samples B and D were annealed in N_2 for 30 min at 850 and 875 °C, respectively, which are optimum annealing temperatures for their Er PL. From Fig. 6(a), one can see that the PL spectra originating from the SRSO matrix of samples B and D are different, the major emission band of sample D is located at around 450 nm with small features present at around 520–540 nm, and the emissions at longer wavelengths of the spectrum are less evident than that of sample B. The 450 nm band has also been attributed to ODC defects but the 520–540 nm structure has been linked to the transition between Er^{3+} excited states and the ground state ($^4S_{3/2} \rightarrow {}^4I_{15/2}$).[31] If we assume that the emission intensity is proportional to the film thickness and normalize the thickness of sample D to that of sample B, the intensity of the SRSO emissions from sample D would be about three times as strong as that from sample B. Figure 6(b) shows the Er PL spectra of the two samples. The full width at half maximum of the spectrum of sample B is 43 nm while that for sample D is 37 nm. The different widths of the Er PL spectra indicate that the Er^{3+} ions lie in somewhat different chemical environments. After normalizing the thickness of sample D to that of sample B, the maximum Er PL intensity of sample B is about 67% stronger than that of sample D. It should be noted that for the two samples annealed at the above temperatures—but in FG—for 1 h, after the same normalization, the Er PL from sample B is about two times stronger in intensity than that from sample D.

Franzò *et al.*[45] discussed the role of Si excess in the PL properties of Er-SRSO grown by PECVD+implanted Er ions, and suggested that when Er is excited through an energy transfer from Si-ncls (i.e., nonresonant excitation), the Er emission at 1.54 μm increases with increasing Si content.

They observed that the Er PL intensity of an Er-SRSO sample with a Si concentration of 44 at. % is about five times stronger than that of a sample with a Si concentration of only 35 at. %. The 325 nm He—Cd laser line employed in our experiments is a nonresonant excitation for the Er^{3+} ions, however, a simple comparison of the Er PL intensities of samples B and D shows that our results are not in agreement with their observations. This discrepancy could be due to our samples B and D being deposited with different techniques. We believe that hydrogen has been incorporated in both samples during their deposition but possibly exists in different Si—H_x bonds, and hydrogen passivation effects play significant role in improving the Er PL intensity as well as Si excess. From our FTIR spectra, hydrogen possibly exists in sample B mainly in the form of Si—H bonds, while in sample D it is supposed to exist in the form of Si—H_2 bonds as well as Si—H bonds from the dissociation of SiH_4.[31] (Note that this is different from that of hydrogenated amorphous Si thin films reported in Ref. 44.) After annealing in FG, the fact that the Er PL from sample B increases further while that from sample D varies little,[18] indicates that the hydrogen passivating efficiency depends on the condition of hydrogen (content, configuration) already existing in the A.D. films. The different hydrogen passivation effects (or efficiency) in the two samples should be responsible for the significant difference in the Er PL. Clearly, further study of the hydrogen chemical states upon deposition and annealing is needed.

IV. CONCLUSIONS

Three Er-doped SRSO films were deposited by using magnetron sputtering in Ar or Ar+H_2 ambients. For the sample grown by Ar sputtering, the excitation of Er^{3+} ions is believed to be a defect-mediated energy transfer process; while for the samples grown by Ar+H_2 sputtering, the defect-related emissions are greatly suppressed and the Er PL at 1.54 μm increases significantly. After annealing in FG ambient, almost no Er PL was observed from the sample grown in an Ar plasma, while the Er PL intensities of the samples grown in Ar+H_2 plasmas increase compared to the cases of annealing in N_2. FTIR spectroscopy showed quite different absorption spectra for the samples dependent on the hydrogen partial pressure during deposition. That the absorption bands are decreasing in intensity after annealing in FG is likely due to fewer Si—O bonds being formed, which suppresses the defect-related emissions and improves the Er PL efficiency by the hydrogen passivation. A comparison of the PL properties with the sample grown by ECR-PECVD indicates that the Er PL efficiency not only depends on the Si excess, but hydrogen content and hydride forms also greatly influence the Er PL. This study is an important contribution to the further understanding of the energy transfer mechanism in the Er-doped SRSO system, which is helpful toward improving the Er PL efficiency.

ACKNOWLEDGMENTS

The authors wish to acknowledge valuable technical support by Jim Garrett (Brockhouse Institute for Materials Research, McMaster University) during the annealing experiments and Steven Kornic (Department of Chemistry, McMaster University) in the FTIR measurements. This work has been supported by the Ontario Research and Development Challenge Fund under the auspices of the Ontario Photonics Consortium.

[1] A. Polman and F. C. J. M. van Veggel, J. Opt. Soc. Am. B **21**, 871 (2004).
[2] A. J. Kenyon, P. F. Trwoga, M. Federighi, and C. W. Pitt, J. Phys.: Condens. Matter **6**, L319 (1994).
[3] G. Franzò, V. Vinciguerra, and F. Priolo, Appl. Phys. A: Mater. Sci. Process. **69**, 3 (1999).
[4] C. E. Chryssou, A. J. Kenyon, T. S. Iwayama, C. W. Pitt, and D. E. Hole, Appl. Phys. Lett. **75**, 2011 (1999).
[5] P. G. Kik, M. L. Brongersma, and A. Polman, Appl. Phys. Lett. **76**, 2325 (2000).
[6] X. D. Pi, O. H. Y. Zalloum, J. Wojcik, A. P. Knights, P. Mascher, A. D. W. Todd, and P. J. Simpson, J. Appl. Phys. **97**, 096108 (2005).
[7] G. Franzò, D. Pacifici, V. Vinciguerra, F. Priolo, and F. Iacona, Appl. Phys. Lett. **76**, 2167 (2000).
[8] J. H. Shin, M. Kim, S. Seo, and C. Lee, Appl. Phys. Lett. **72**, 1092 (1998).
[9] M. Fujii, M. Yoshida, Y. Kanzawa, S. Hayashi, and K. Yamamoto, Appl. Phys. Lett. **71**, 1198 (1997).
[10] X. L. Wu, Y. F. Mei, G. G. Siu, K. L. Wong, K. Moulding, M. J. Stokes, C. L. Fu, and X. M. Bao, Phys. Rev. Lett. **86**, 3000 (2001).
[11] F. Gourbilleau, C. Dufour, M. Levalois, J. Vicens, R. Rizk, C. Sada, F. Enrichi, and G. Battaglin, J. Appl. Phys. **94**, 3869 (2003).
[12] T. Makimura, H. Uematsu, K. Kondo, C. Li, and K. Murakami, Appl. Phys. A: Mater. Sci. Process. **79**, 799 (2004).
[13] J. S. Ha *et al.*, Appl. Phys. A: Mater. Sci. Process. **79**, 1485 (2004).
[14] G. Franzò, S. Boninelli, D. Pacifici, F. Priolo, F. Iacona, and C. Bongiorno, Appl. Phys. Lett. **82**, 3871 (2003).
[15] D. Kuritsyn, A. Kozanecki, H. Przybylińska, and W. Jantsch, Appl. Phys. Lett. **83**, 4160 (2003).
[16] C. Y. Chen, W. D. Chen, S. F. Song, Z. J. Xu, X. B. Liao, G. H. Li, and K. Ding, J. Appl. Phys. **94**, 5599 (2003).
[17] M. Carrada, F. Gourbilleau, C. Dufour, M. Levalois, and R. Rizk, Opt. Mater. (Amsterdam, Neth.) **27**, 915 (2005).
[18] C. L. Heng, O. H. Y. Zalloum, T. Roschuk, D. Blakie, J. Wojcik, and P. Mascher, Electrochem. Solid-State Lett. **10**, K20 (2007).
[19] D. Comedi, O. H. Y. Zalloum, and P. Mascher, Appl. Phys. Lett. **87**, 213110 (2005).
[20] F. Gourbilleau, P. Choppinet, C. Dufour, M. Levalois, R. Madelon, J. Vicens, R. Rizk, and M. Prassas, Mater. Sci. Eng., B **105**, 44 (2003).
[21] C. Ternon, F. Gourbilleau, X. Portier, P. Voivenel, and C. Dufour, Thin Solid Films **419**, 5 (2002).
[22] A. Anedda, R. Boscaino, M. Cannas, R. Corpino, F. M. Gelardi, and M. Leone, Nucl. Instrum. Methods Phys. Res. B **116**, 360 (1996).
[23] C. Barthou, P. H. Duong, A. Oliver, J. C. Cheang-Wong, L. Rodrfguez-Fernández, A. Crespo-Sosa, T. Itoh, and P. Lavallard, J. Appl. Phys. **93**, 10110 (2003).
[24] H. Nishikawa, E. Watanabe, D. Ito, M. Takiyama, A. Ieki, and Y. Ohki, J. Appl. Phys. **78**, 842 (1995).
[25] L. S. Liao, X. M. Bao, N. S. Li, X. Q. Zheng, and N. B. Min, J. Lumin. **68**, 199 (1996).
[26] A. Wellner, V. Paillard, H. Coffin, N. Cherkashin, and C. Bonafos, J. Appl. Phys. **96**, 2403 (2004).
[27] G. Ghislotti, J. Electrochem. Soc. **144**, 2196 (1997).
[28] A. Kozanecki, B. J. Sealy, K. Homewood, S. Ledain, W. Jantsch, and D. Kuritsyn, Mater. Sci. Eng., B **81**, 23 (2001).
[29] L. Rebohle, J. von Borany, H. Fröb, and W. Skorupa, Appl. Phys. B: Lasers Opt. **71**, 131 (2000).
[30] L. N. Skuja and A. R. Silin, Phys. Status Solidi A **56**, K11 (1979).
[31] C. L. Heng, O. H. Y. Zalloum, J. Wojcik, T. Roschuk, and P. Mascher, J. Appl. Phys. **103**, 024309 (2008).

[32]G. Allan, C. Delerue, and M. Lannoo, Phys. Rev. Lett. **78**, 3161 (1997).
[33]D. Pacifici, E. C. Moreira, G. Franzò, V. Martorino, F. Priolo, and F. Iacona, Phys. Rev. B **65**, 144109 (2002).
[34]M. I. Alayo, I. Pereyra, W. L. Scopel, and M. C. A. Fantini, Thin Solid Films **402**, 154 (2002).
[35]F. Ay and A. Aydinli, Opt. Mater. (Amsterdam, Neth.) **26**, 33 (2004).
[36]D. V. Tsu, G. Lucovsky, and B. N. Davidson, Phys. Rev. B **40**, 1795 (1989).
[37]P. G. Pai, S. S. Chao, Y. Takagi, and G. Lucovsky, J. Vac. Sci. Technol. A **4**, 689 (1986).
[38]A. R. Wilkinson and R. G. Elliman, J. Appl. Phys. **96**, 4018 (2004).
[39]X. D. Pi, P. G. Coleman, R. Harding, G. Davies, R. M. Gwilliam, and B. J. Sealy, Physica B **340–342**, 1094 (2003).
[40]S. J. Patil and S. A. Gangal, J. Micromech. Microeng. **15**, 1956 (2005).
[41]L. N. He, T. Inokuma, and S. Hasegawa, Jpn. J. Appl. Phys., Part 1 **35**, 1503 (1996).
[42]R. Guo, Y. Kurata, T. Inokuma, and S. Hasegawa, J. Non-Cryst. Solids **351**, 3006 (2005).
[43]Z. Yu, M. Aceves-Mijares, E. Quiroga, R. Lopez-Estopier, J. Carrillo, and C. Falcony, J. Appl. Phys. **100**, 013524 (2006).
[44]M. Hossain, H. H. Abu-Safe, H. Naseem, and W. D. Brown, J. Non-Cryst. Solids **352**, 18 (2006).
[45]G. Franzò, E. Pecora, F. Priolo, and F. Iacona, Appl. Phys. Lett. **90**, 183102 (2007).